Desalination and Water Treatment
www.deswater.com

doi:10.5004/dwt.2017.21033

83 (2017) 168–175
July

Lignosulfonate-based ternary nanocomposite hydrogels for efficient textile dye absorption

Zhili Zhang, Rendang Yang*, Wenhua Gao, Kefu Chen

State Key Laboratory of Pulp & Paper Engineering, South China University of Technology, Guangzhou 510640, China, Tel. +86 020 87110084, Fax +86 020 87110084, email: qhxyzhangzhili@163.com (Z. Zhang), rdyang@scut.edu.cn (R. Yang), segaowenhua@scut.edu.cn (W. Gao), ppchenkf@scut.edu.cn (K. Chen)

Received 21 December 2016; Accepted 12 June 2017

ABSTRACT

In the present study, a new solid adsorbent, lignosulfonate-graphene oxide-acrylamide (LS-GO-AM) ternary composite hydrogel possessing good mechanical strength and high dye adsorption capacity, was prepared by a simple polymerization, and used for the removal of dyes from aqueous solution. The adsorption property of a model dye, methylene blue (MB), onto the hydrogel was studied. The effects of adsorption time, initial pH, and concentration were investigated. When the initial MB concentration was 3 $mg \cdot L^{-1}$ at an LS-GO-AM concentration of 4 $g \cdot L^{-1}$, the absorption was 98.36% while the solution was nearly decolorized. Moreover, adsorption kinetic and equilibrium data were described well with pseudo-second-order and Langmuir isotherm models for MB adsorption. The LS-GO-AM composite hydrogel with enhanced mechanical strength could be easily separated from the reaction system.

Keywords: Lignosulfonate; Graphene oxide; Hydrogels; Adsorption

1. Introduction

More and more attention has been paid to effluent dyes from textile, leather, paper, and plastics. Various techniques such as physical, chemical, physicochemical and biological treatments are available for dye-containing wastewater treatment [1]. In these methods, adsorption has been considered to be superior to other techniques to remove dyes due to its lower operating cost, convenience of design, and effective elimination of the secondary contamination [2].

Lignin is one of the most abundant renewable resources whose content in wood varies from 19 to 35%. Some of lignin-based materials were used adsorbent for color removal and the results have shown that through lignin chemical modification, the use of lignin as an adsorbent for dye removal from aqueous media can be significantly enhanced [3]. Lignosulfonate is a modified lignin obtained from spent sulfite pulping liquors that contains many hydrophilic groups (sulfonic, phenylic hydroxyl and alcoholic hydroxyl) [4], to promote surface adsorption [5], and demonstrate great potential in wastewater treatment. In recent years, great academic interest has been devoted to investigate the lignosulfonate-based adsorbents [6,7]. But lignosulfonate is difficult to collect from water due to its solubility; therefore, it is crucial that a lignosulfonate-based sorbent material be easily separated from the reaction system [8]. Although the chemical reactivity of lignin is low, lignin can graft-copolymerize with vinyl monomers such as acrylic acid and acrylamide to make a polymeric hydrogel [9]. Compared with lignin, lignosulfonate possesses better chemical reactivity to prepare hydrogel with high dyes adsorption capacities.

Graphene sheets—one-atom-thick two-dimensional layers of sp^2-bonded carbon—have inspired ever-increasing enthusiasm recently owing to its exceptional chemical and mechanical property values such as its 1 TPa Young's modulus and 130 GPa ultimate strength [10]. Graphene oxide, a graphene precursor, has a large surface area that can accommodate many oxygen-containing hydrophilic functional groups such as –COOH and –OH. The presence of these functional groups makes graphene oxide sheets strongly hydrophilic, allowing it to readily swell and disperse in

*Corresponding author.

1944-3994 / 1944-3986 © 2017 Desalination Publications. All rights reserved.

water [11]. Furthmore, these reactive groups on the surface of GO provide good compatibility with polymers to form a GO/polymer composite with a stable structure [12]. In addition, these groups have strong sorbent ability for removal of dyes from aqueous solutions [8,13]. Nevertheless, the hydrophily of GO tend to form hydrogen bonding interaction between water molecules and GO, which make it hard separated from the reaction system.

Therefore, if the mechanical strength of lignosulfonate hydrogels was improved, an adsorbing material with high dyes adsorption capacity could be separated from the reaction system. In this work, a new solid adsorbent, lignosulfonate-graphene oxide-acrylamide ternary composite hydrogel, was prepared by simple solution polymerization for the removal of dyes.

2. Materials and methods

2.1. Materials

Lignosulfonate ($C_{20}H_{24}Na_2O_{10}S_2$, MW 534.51) was obtained from Shanghai Macklin Biochemical Co., Ltd. Acrylamide (AM), N, N′-methylenebisacrylamide (MBA), methylene blue (MB) and graphite powder (purity of 99.95%) were purchased from Aladdin Industrial Corporation (China). $KMnO_4$, concentrated H_2SO_4, concentrated HCl, $CaCl_2$, 30% H_2O_2 and other reagents were of analytical grade and used without further purification.

2.2. Methods

2.2.1. Synthesis of GO and LS-GO-AM ternary composite hydrogel

GO was synthesized from natural graphite powder using a modified Hummers's method [14]. Ternary composite hydrogels were prepared by a simple solution polymerization using solutions consisting of monomers (Ls, AM and GO), crosslinker (MBA), and initiator (H_2O_2-$CaCl_2$). First, 2.50 mg prepared GO was dispersed in 5 mL of deionized water in a 50 mL glass flask under ultrasonication (220 V, 200W) for 2 h. Subsequently, 0.40 g LS and 0.30 g $CaCl_2$ was added to the GO suspension and stirred vigorously to form a mixture. Then 4.8 g AM, 0.07 g MBA, and 60 µL of 30% H_2O_2 were added. The ternary system (LS-GO-AM) was stirred at room temperature until it became a stable suspension. The homogeneous mixture solutions were transferred into a glass tube and kept for hydrogel formation under nitrogen at 50°C for 10 h without stirring. After hydrogel formation, the ternary composite hydrogels, in their existing form, were taken out of the glass tube and put into deionized water to remove homopolymers and unreacted monomers. LS-AM hydrogels were prepared by the same method.

2.2.2. Characterization

Fourier transform infrared spectroscopy spectra (FT-IR) was recorded on a VERTEX 70 (Bruker, German) over 500-4000 cm^{-1} at a resolution of 0.5 cm^{-1}. XRD was determined by a D8 ADVANCE X-ray diffractometer under the following conditions: tube current and voltage were 20 mA and 30 kV, respectively, Cu target, and data were collected over the 2θ Bragg angles of 5–90 at a scanning speed of 0.02° s^{-1}. The thermal stability of the samples was evaluated using thermogravimetric analysis (TGA) (TGA Q500, TA, USA). Samples of approximately 12 mg weight were heated in an aluminum crucible to 700°C at a heating rate of 20°C min^{-1} while the apparatus was continually flushed with a nitrogen flow of 25 mL min^{-1}. Tensile testing of the hydrogel samples with length of ~10 mm were measured using an INSTRON 5565 universal testing equipment with a test speed of 1 mm·min^{-1}. The relative humidity of 52% and temperature of 23°C were kept during the measurement. At least five specimens were used for each sample in the test and averaged. The morphology of the surfaces of the hydrogels were observed by a scanning electron microscopy (Bruker, German) at 10 kV. The samples were spread on a circular base with double sided tape that has high conductivity and covered with a thin layer of gold (about 2 nm) by sputtering to promote conductivity before SEM observation.

2.2.3. Absorption of MB by LS-GO-AM ternary composite hydrogel

The effects of adsorption time, initial MB concentration, and pH value on adsorption for ternary composite hydrogels were carried out by single factor. The MB stock solution was prepared by dissolving methylene blue powder in deionized water, and the desired pH value was adjusted using 0.1 mol·L^{-1} HCl or 0.1 mol·L^{-1} NaOH solution. Typically, a test solution containing MB and dry hydrogel were loaded in a 200 mL conical flask and placed it in air table with 200 rpm stirring speed at 25°C for 24 h to reach equilibrium. After a desired adsorption time, the hydrogel was removed with forceps, while the concentration of MB after adsorption was measured by testing the absorbance at 664 nm (Fig. 1). A diode array spectrophotometer (Model-8453, Agilent Technologies, Inc, USA) was employed for the spectrophotometric measurements.

The adsorbed amount of MB on the adsorbent was calculated according to the following equations:

$$Q = (C_0 - C_e) \times \frac{V}{m} \quad (1)$$

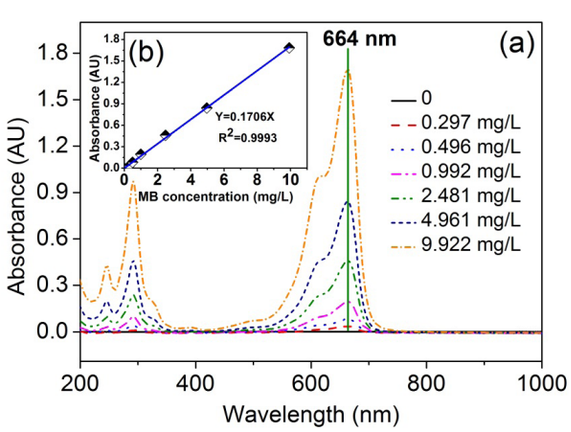

Fig. 1. Absorption spectrum (a) and standard curve (b).

$$q = \frac{(C_0 - C_e)}{C_0} \times \% \quad (2)$$

where Q is the adsorption capacity (mg·g^{-1}); C_0 and C_e are the MB concentration before and after adsorption (mg·L^{-1}), respectively; V is the initial volume of the MB solution (mL); m is the weight of the hydrogel (g); and q is the adsorptivity (%).

2.2.4. Desorption process

The desorption process was conducted to employ aqueous alcohol solutions (water: ethanol = 1:1, v/v) washing for several times. Acidify the aqueous alcohol solutions with1 mol·L^{-1} HCl to pH 2.

3. Results and discussion

3.1. FTIR analysis

Fig. 2 shows the FT-IR spectra of GO, LS, LS-AM and LS-GO-AM hydrogels. As-prepared GO sheets show characteristic FT-IR peaks at 3400 cm^{-1}, 1720 cm^{-1}, 1620 cm^{-1}, 1200 cm^{-1} and 1061 cm^{-1} to O–H (broad-coupling hydroxyl group), C=O groups, C–C bonds, C–O–C and C–O groups, respectively [15]. The characteristic peaks located at 3408 cm^{-1}, assigned to O–H stretching of LS indicating the presence of phenol and aliphatic hydroxyls. Peaks 1219 cm^{-1} and 1040 cm^{-1} indicated that LS contained sulfonic acid groups. The bands at 618 cm^{-1} corresponded to the C–S stretching vibration [16]. Compared to the original LS, a new peak at 3200 cm^{-1} appeared for the LS-AM and LS-AM-GO hydrogels, which was the stretching band of the N–H bonds, that confirmed successful functionalization of LS chains onto AM. Additionally, compared with the LS-AM hydrogel, the C–O stretching vibration peak at 1719 cm^{-1} belonging to GO is weak in the LS-GO-AM hydrogel, indicating the existence of GO. There was a broad peak at ~3427 cm^{-1} suggesting the hydrogen bonds are disturbed in the LS-GO-AM hydrogel and the change could be ascribed to the strong interaction through hydrogen bonds between LS-AM hydrogels and GO [17]. So the FT-IR results confirmed the proposed formation of LS-GO-AM hydrogels.

3.2. XRD analysis

Compared with pristine graphite, the characteristic 2θ peak of GO sheets appearing at ~10.7°corresponds to the (001) interplanar spacing of 0.83 nm caused by the oxygen-rich groups on both sides of the sheets and the water molecules trapped between the sheets [18]. For LS, the broad and low intensity diffraction peak between 20° and 30° can be attributed to the (002) diffraction peak of carbon, indicative of its low graphitization and amorphous nature [19]. After loading GO sheets with the LS-AM hydrogel, the strong peak of GO at 10.7° almost disappeared. It was noted that incorporation of a small handful of GO only slightly increased the intensity of the characteristic peaks of LS-AM hydrogel [20]. The insignificant pick of GO in XRD patterns indicates that the interaction between lignosulfonate and GO forms a heterogeneous structure [21].

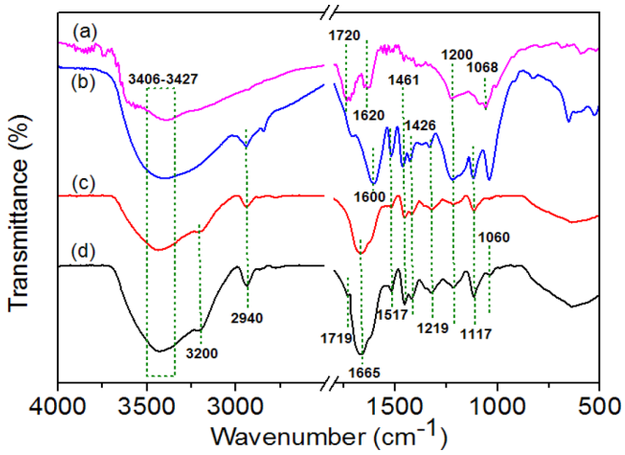

Fig. 2. FT-IR spectras of GO (a), LS (b), LS-AM (c) and LS-GO-AM hydrogels (d).

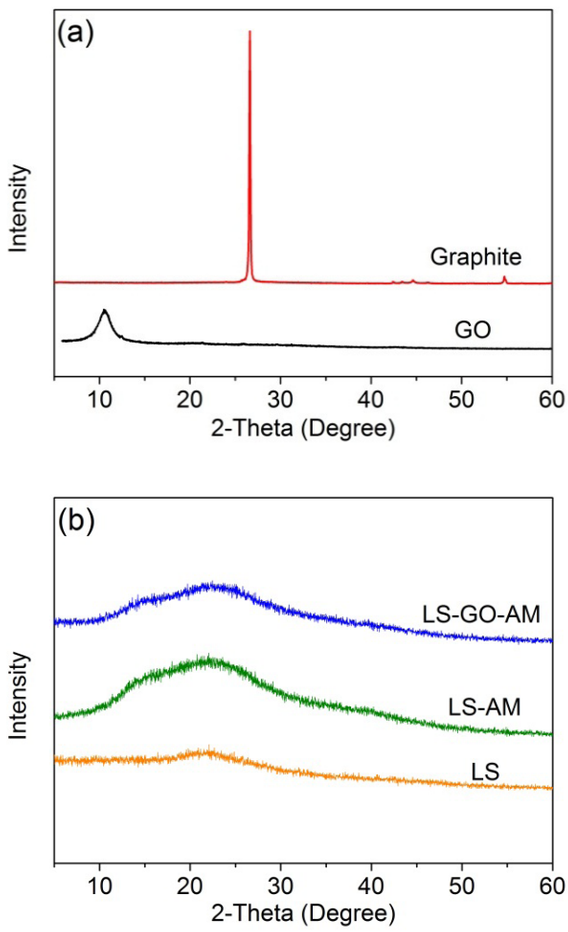

Fig. 3. XRD patterns of graphite, GO, LS, LS-AM and LS-GO-AM hydrogels.

3.3. TGA analysis

To test the thermal stability of the hydrogels before and after the addition of GO sheets, the samples were examined by TGA and DTG. TGA traces of pristine graphite showed a negligible weight loss over the entire temperature range. GO sheets were thermally unstable and started to display sharp weight losses owing to decomposition of oxygen-containing groups in GO at 150–240°C [22]. In the TGA curve of the lignosulfonate, the degradation was observed to start around 175°C and almost 30% weight loss occurred at 300°C [23]. No obvious weight loss peak of lignosulfonate was observed. In Fig. 4(a), the degradation of pure LS-AM hydrogel began at ~ 260°C. The rate of weight loss increased with temperature from 200 to 420°C and thereafter decreased to attain a maximum degradation temperature (T_{max}) of 374.4°C while the T_{max} of LS-GO-AM ternary composite hydrogel was 383.5°C. The T_{max} of LS-GO-AM ternary composite hydrogel was higher than that of LS-AM hydrogel. From the temperature of maximum weight loss rate, it was found that since GO sheets accession to the LS-AM hydrogel, the thermal stability of the composite hydrogel significantly improved. The increase in the thermal stability of LS-GO-AM hydrogel could be ascribed to an effective attachment of lignosulfonate to the GO sheets that constrains the segmental motion of the lignosulfonate by hydrogen bonding, as demonstrated in other reports [24,25].

3.4. Tensile testing

Fig. 5 shows the typical stress-strain curves (a) and Young's modulus (b) of LS-AM and LS-GO-AM ternary composite hydrogels. As shown, the mechanical properties of the composite hydrogel containing a small amount of GO can be remarkably increased. The LS-AM hydrogel was broken under pressure due to its poor toughness, while the LS-GO-AM hydrogel maintained a better shape. In addition, the LS-GO-AM hydrogel could quickly recover its original shape once the compression force was removed. Indeed, a small amount of GO could significantly improve the mechanical properties of composites. In Fig. 5, the tensile strength of LS-GO-AM ternary composite hydrogel increased 285.3% (18.23 → 70.24 Pa). The Young's modulus of LS-AM and LS-GO-AM ternary composite hydrogel were obtained by measuring the slope in the linear region of the stress-strain curve [26]. In Fig. 5b, the Young's modulus of LS-GO-AM ternary composite hydrogel reached

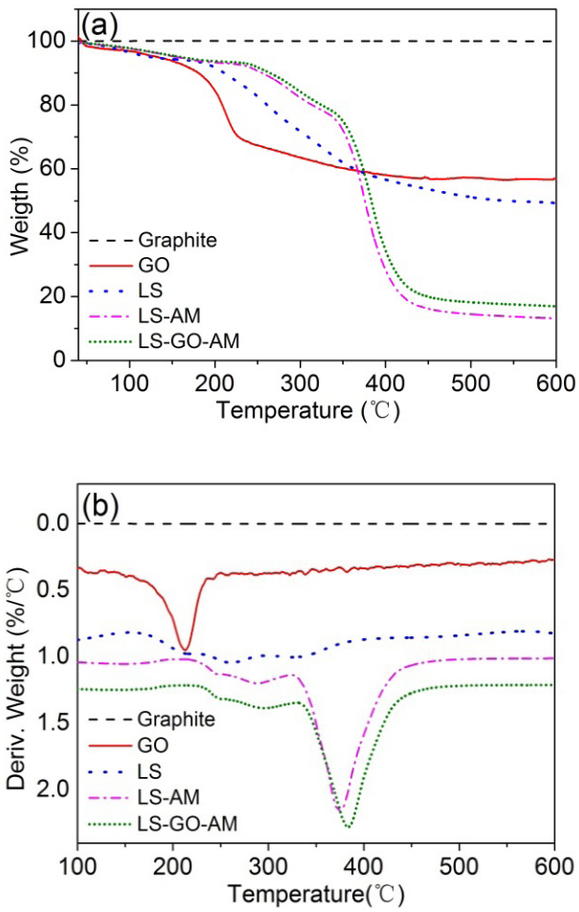

Fig. 4. TGA (a) and DTG (b) curves of Graphite, GO, lignosulfonate, LS-AM and LS-GO-AM hydrogels.

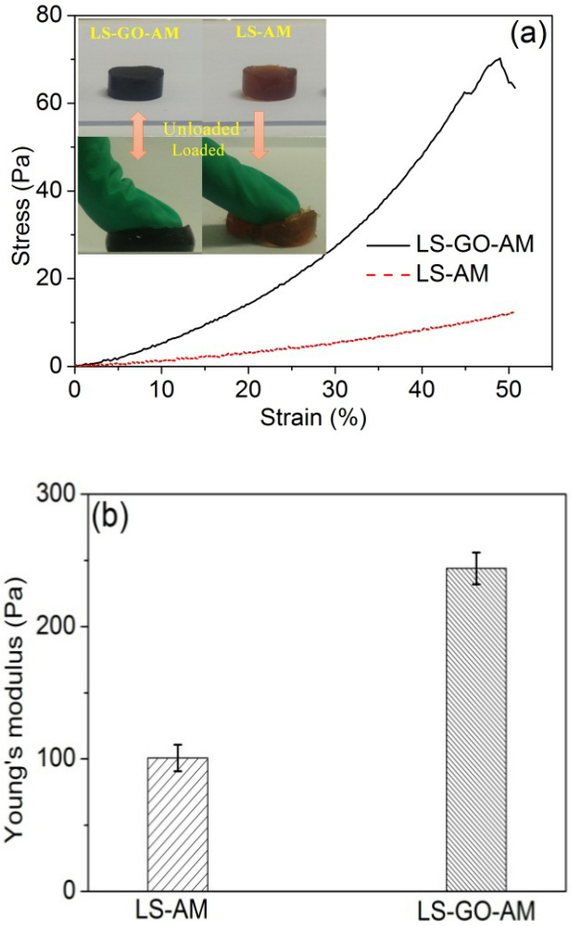

Fig. 5. Stress-strain behaviors (a) and Young's modulus (b) of LS-AM and LS-GO-AM ternary composite hydrogels.

244.01 Pa with GO sheets addition, and increased 142.1% relative to the LS-AM hydrogel. This may be because that the uniformly dispersed GO/LS-AM hydrogel had a typical 3D network structure and the residual graphene nanoplates were evenly distributed within that matrix and strong interfacial adhesion between graphene oxide and lignosulfonate were obtained [27]. The special structure also improved the mechanical properties [28].

3.5. SEM

SEM images were used to investigate the structure of LS-AM and LS-GO-AM that show a loose 3D network structure with pore sizes of several micrometers to tens of micrometers. There are more pores on the surface of LS-GO-AM as compared to LS-AM. This was because GO sheets reduce the expansion of the gel matrixes resulting in a decrease in the pore sizes [29]. The porous materials have a local unidirectional porous structure that facilitates diffusion of MB. Unfortunately, there are also a small number of closed pores in the surfance of hydrogels, which were not helpful to the adsorption process due to the low gas permeability [30,31]. The possible reason, due to the reduction in volume during the freeze drying, a handful of pores were closed. The existence of pore sizes increases the surface area of porous material, so more functional groups are exposed [32].

3.6. Adsorption of MB

The effect of adsorption time on the adsorption of MB onto the LS-GO-AM ternary composite hydrogel is shown in Fig. 7a. When the adsorption time was increased, the adsorption capacity and absorption increased substantially. When the adsorption time is 5 h, the absorption is 56%, whereas the adsorption capacity reaches 17.30 mg·g^{-1}. Due to the slow diffusion of adsorbate molecules in the hydrogel, the LS-GO-AM ternary composite hydrogel exhibited remarkably slower adsorption kinetics than other adsorbents [33]. Moreover, the equilibrium balance of adsorption was reached at 7 h, in which a higher adsorption capacity was obtained, and the adsorption capacity and adsorptivity reached 18.09 mg·g^{-1} and 59%, respectively. The surface charge of the LS-GO-AM hydrogel, the ionization of GO [34], lignosulfonate and acrylamide [35] as well as the structure of the MB molecules were affected by the pH value, so it has significant influence on the absorption process. In Fig. 7b, at a MB concentration of 120 mg/L, the absorption capacity increases to 18.25 mg·g^{-1} at pH 7. The LS-GO-AM hydrogel was protonated in acid region, due to the competitions among the excessive H^+ ions on the surface of hydrogel and water, the absorbing ability was reduced greatly. However, the hydrogel was deprotonated in alkaline region, and the electrostatic interaction between hydrogel and MB molecules increases resulting in a higher dye adsorption. Similarly, the pH-regulated absorption behavior is also observed in other carbon absorbents [36]. In Fig. 7c the absorption decreased while adsorption capacity revealed a general upward trend. Because there is an insufficient amount of the LS-GO-AM ternary composite hydrogel to adsorb MB, there appears saturation. When the initial MB concentration is 3 mg·L^{-1}, the absorption is up to 98.36% and the solution can be nearly decolorized. Furthermore, when the initial MB concentration is 700 mg·L^{-1}, the adsorption capacity and absorption are 47.52 mg·g^{-1} and 34.04%, respectively. Quantitatively, the adsorption capacities and absorption of LS-AM was 34.24 mg·g^{-1} and 21.15%, respectively. Obviously, the capacities and adsorptivity of LS-GO-AM was significantly improved. Compared with GO and lignosulfonate, LS-GO-AM hydrogels with better thermal stability and mechanical properties could be easily separated from the reaction system, thus to promote industrialization. The results also show that the dye absorption of LS-GO-AM ternary composite hydrogel are higher than modified lignin [3,37].

Photographs of the MB solution before and after the LS-GO-AM ternary composite hydrogel treatment were visually compared as shown in Fig. 7d. Reduction in decreasing degree of color was observed with the MB concentration increased. Because there is no enough composite hydrogel to adsorb MB, while when the initial MB concentration was low, the solution was nearly decolorized.

3.7. Adsorption kinetics

Pseudo-first-order [Eq. (3)] and pseudo-second-order [Eq. (4)] models were employed to fit the experimentally obtained adsorption data [38]. Pseudo-first-order and pseudo-second-order equation may be expressed as:

$$\ln(Q_e - Q_t) = \ln Q_e - k_1 t \tag{3}$$

$$\frac{t}{Q_t} = \frac{1}{k_2 Q_e^2} + \frac{t}{Q_e} \tag{4}$$

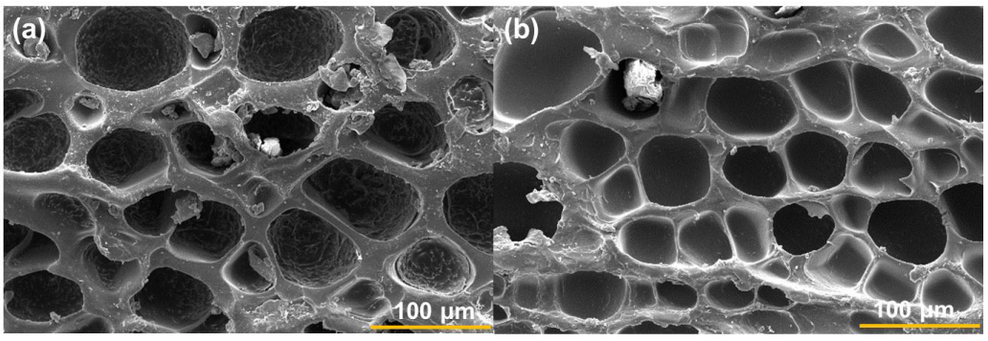

Fig. 6. SEM images of hydrogel samples: (a) LS-AM hydrogel; (b) LS-GO-AM composite hydrogels.

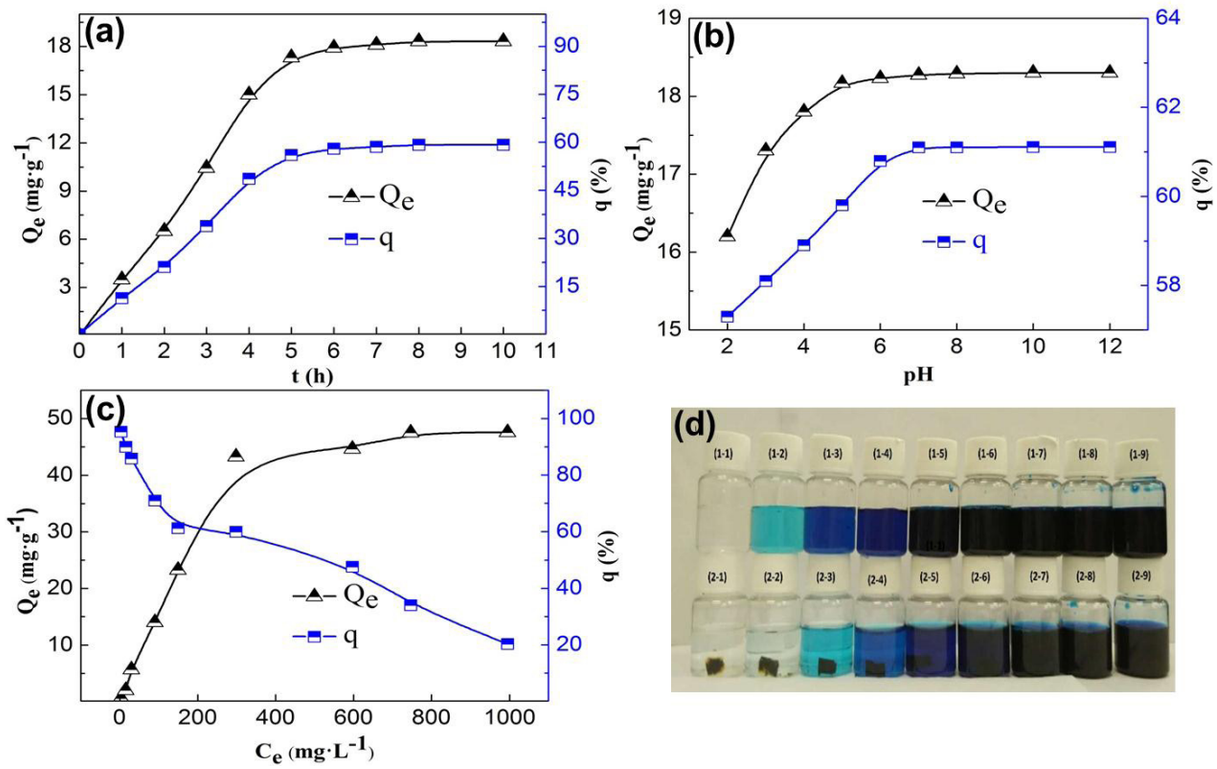

Fig. 7. Adsorption behaviors of MB on LS-GO-AM ternary composite hydrogel. (a) Effect of the adsorption time (C_0 = 120 mg/L, T = 25°C, pH = 7.0). (b) Effect of the initial pH value (C_0 = 120 mg/L, T = 25°C, t = 7 h). (c) Effect of the initial MB concentration (T = 25°C, pH = 7.0, t = 7 h). (d) photographs of the MB solution before (top) and after (bottom) the LS-GO-AM ternary composite hydrogel treatment.

where k_1 and k_2 are the pseudo-first-order and pseudo-second-order rate constant. Q_t is the amounts of MB adsorbed per adsorbent (mg·g^{-1}) at time t. The parameters of the pseudo-first-order and pseudo-second-order equations for the adsorption of MB onto LS-GO-AM ternary composite hydrogel are listed in Fig. 8a and Table 1.

As can been seen from Fig. 8a and Table 1, these two models both have high correlation coefficients, but the calculated data according to the pseudo-first-order equation did not agree with the experimental adsorption capacity (Q_e). The numerical results calculated from pseudo-second-order equation are close to the measured data which indicated that the pseudo-second-order model was a more applicable model to the kinetics of MB adsorption. Thus, we can infer that the removal of MB by the LS-GO-AM ternary composite hydrogel is mainly controlled by the chemical interaction between MB and the binding sites [24].

3.8. The adsorption isotherm

Both Langmuir and Freundlich isotherm models were used to describe and analyze adsorption equilibrium as described by Eqs. (5) and (6) [38]:

$$\frac{C_e}{Q_e}=\frac{C_e}{Q_m}+\frac{1}{K_L Q_m} \quad (5)$$

Table 1
Kinetic parameters and adsorption isotherm parameters for the adsorption of MB onto LS-GO-AM ternary composite hydrogel

Pseudo-first-order model			Pseudo-second-order model		
Q_e (mg·g^{-1})	k_1 (L·mg^{-1})	R^2	Q_e (mg·g^{-1})	k_2	R^2
24.63	0.1227	0.9858	18.24	6.386×10^{-3}	0.9969
Langmuir isotherm model			Freundlich isotherm model		
Q_m (mg·g^{-1})	K_L (L·mg^{-1})	R^2	K_F (mg·g^{-1})	$1/n$	R^2
45.45	0.0498	0.9901	1.681	0.5195	0.9480

$$\ln Q_e=\frac{1}{n}\ln C_e+\ln K_F \quad (6)$$

where Q_e is the amount of MB adsorbed (mg·g^{-1}) at equilibrium, Q_m (mg·g^{-1}) and K_L are the Langmuir constants related to the saturated adsorption capacity and adsorption energy, respectively. K_F and n were the Freundlich constants related to the sorption capacity and sorption intensity, respectively. The fitted line and corresponding parameters for the sample obtained from the lines are listed in Fig. 8b and Table 1. In Table 1 the absorption

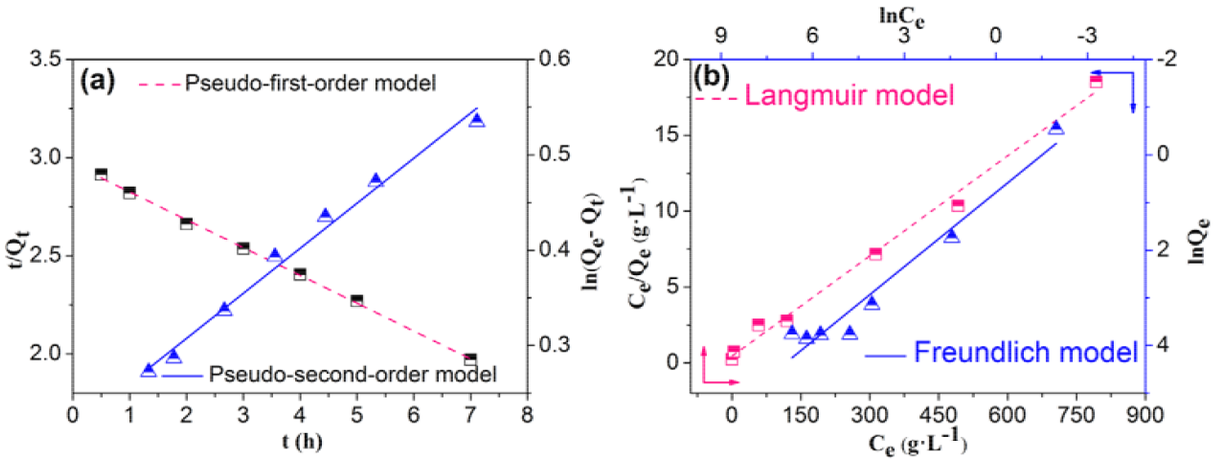

Fig. 8. (a) Fitting results for the pseudo-first-order and pseudo-second-order kinetic models (C_0 = 120 mg/L, T = 25°C, pH = 7.0). (b) Fitting results for the Langmuir and Freundlich isotherm models (T = 25°C, pH = 7.0, t = 7 h).

data of MB onto LS-GO-AM ternary composite hydrogel can be fitted by the Langmuir absorption isotherm model with a high higher correlation coefficient (0.99) compared to the Freundlich model. In addition, the experimental adsorption capacity for the adsorption of Q_m was 45.45 mg/g, very near to the value calculated from Langmuir model Q_m 47.52 mg/g. It was shown that the equilibrium adsorption of LS-GO-AM ternary composite hydrogels were well described by the Langmuir isotherm model, indicating that the adsorption process was mainly governed at the monolayer and took place on a homogeneous surface.

3.9. Application of LS-GO-AM hydrogel

In order to improve the adsorption efficiency of LS-GO-AM hydrogel, thus to promote industrialization, we fabricated a simple device for removing MB from dyeing wastewater (Fig. 9). The volume of feeding solution was 50 mL and the initial concentration of MB was 120 mg/L. The LS-GO-AM hydrogel is 2 cm in length deep and has a diameter of 1 cm. And the flow was adjusted of 1 mL·min^{-1}. When the adsorption time is 50 min, the adsorption capacity reaches 25.7 mg·g^{-1}. This device has the advantage of simple techniques, convenient operation, and the continuous operation could be realized. Furthermore, the LS-GO-AM hydrogels could be regenerated and reused after several recycled adsorption-desorption processes, and the adsorption capacities maintained ~ 97% after 5 cycles and ~ 90% after 10 cycles.

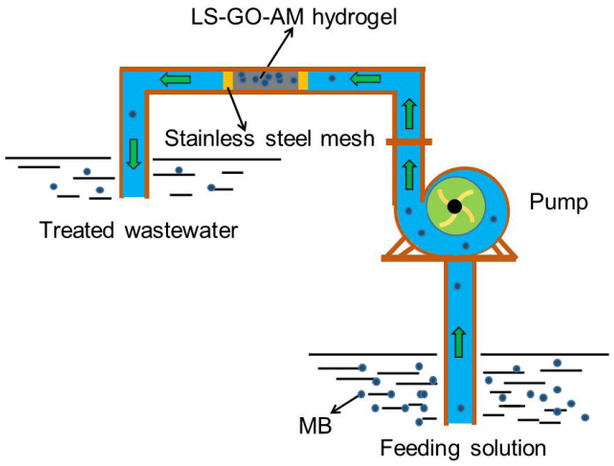

Fig. 9. Schematic diagram of the device.

4. Conclusions

LS-GO-AM ternary composite nanocomposites hydrogels were synthesized by simple solution polymerization. Compared with LS-AM hydrogels, the thermal stability and mechanical properties of the composite hydrogels were significantly improved. The equilibrium adsorption isotherm reveals that the Langmuir model describes the adsorption process better. Additionally, the LS-GO-AM ternary composite hydrogel displayed enhanced mechanical strength and could be easily removed from the reaction system. The results showed that the LS-GO-AM ternary composite hydrogel has great potential application in removal of dyes (MB) from industrial wastewater. Importantly, the adsorption capacities maintained ~ 97% after 5 cycles and ~ 90% after 10 cycles.

Acknowledgments

The authors are grateful for the financial support afforded by State Key Laboratory of Pulp and Paper Engineering, China (2015ZD04, 2016QN01), the National Natural Science Foundation of China (31400512), 111 plan and Guangdong provincial science & technology plan projects (2015B020241001).

References

[1] E. Forgacs, T. Cserhati, G. Oros, Removal of synthetic dyes from wastewaters: a review, Environ. Int., 30 (2004) 953–971.

[2] L. Sun, H. Yu, B. Fugetsu, Graphene oxide adsorption enhanced by in situ reduction with sodium hydrosulfite to remove acridine orange from aqueous solution, J. Hazard. Mater., 203 (2012) 101–110.

[3] N.C. Filho, E.C. Venancio, M.F. Barriquello, A.A.W. Hechenleitner, E.A.G. Pineda, Methylene blue adsorption onto modified lignin from sugar cane bagasse, Eclética Química, 32 (2007) 63–70.

[4] G. Gupta, N. Birbilis, A.B. Cook, A.S. Khanna, Polyaniline-lignosulfonate/epoxy coating for corrosion protection of AA2024-T3, Corros. Sci., 67 (2013) 256–267.

[5] Q.F. Lü, J.Y. Zhang, Z.W. He, Controlled preparation and reactive silver-ion sorption of electrically conductive poly (n-butylaniline)-lignosulfonate composite nanospheres, Chem-Eur. J., 18 (2012) 16571–16579.

[6] M.A. Zulfikar, E.D. Mariske, S.D. Djajanti, Adsorption of lignosulfonate compounds using powdered eggshell, Songklanakarin J. Sci. Technol., 34(3) (2012) 309–316.

[7] M.H. Liu, J.H. Huang, Removal and recovery of cationic dyes from aqueous solutions using spherical sulfonic lignin adsorbent, J. Appl. Polym. Sci., 101(4) (2006) 2284–2291.

[8] Y. Chen, L. Chen, H. Bai, L. Li, Graphene oxide–chitosan composite hydrogels as broad-spectrum adsorbents for water purification, J. Mater. Chem., A1 (2013) 1992–2001.

[9] Y.X. Wu, J.H. Zhou, C.C. Ye, H.Z. Sun, R.J. Zhao, Optimized synthesis of lignosulphonate-gpoly (acrylic acid-co-acrylamide) superabsorbent hydrogel based on the taguchi method, Iran. Polym. J., 19 (2010) 511–520.

[10] C. Lee, X. Wei, J.W. Kysar, J. Hone, Measurement of the elastic properties and intrinsic strength of monolayer graphene, Science, 321 (2008) 385–388.

[11] S. Stankovich, D.A. Dikin, G.H. Dommett, K.M. Kohlhaas, E.J. Zimney, E.A. Stach, R.S. Ruoff, Graphene-based composite materials, Nature, 442 (2006) 282–286.

[12] L. Jiang, X.P. Shen, J.L. Wu, K.C. Shen, Preparation and characterization of graphene/poly (vinyl alcohol) nanocomposites, J. Appl. Polym. Sci., 118 (2010) 275–279.

[13] R.B. Wang, R.D. Yang, B. Wang, W.H. Gao, Efficient degradation of methylene blue by the nano TiO_2-functionalized graphene oxide nanocomposite photocatalyst for wastewater treatment, Water Air Soil Poll., 227(1) (2016) 2.

[14] W.S. Hummers Jr, R.E. Offeman, Preparation of graphitic oxide, J. Am. Chem. Soc., 80 (1958) 1339–1339.

[15] N.D. Luong, N. Pahimanolis, U. Hippi, J.T. Korhonen, J. Ruokolainen, L.S. Johansson, J. Seppälä, Graphene/cellulose nanocomposite paper with high electrical and mechanical performances, J. Mater. Chem., 21 (2011) 13991–13998.

[16] L. Shao, J.H. Qiu, H.X. Feng, M.Z. Liu, G.H. Zhang, J.B. An, H.L. Liu, Structural investigation of lignosulfonate doped polyaniline, Synthetic Met., 159 (2009) 1761–1766.

[17] Y. Liu, M. Park, H.K. Shin, B. Pant, J. Choi, Y.W. Park, H.Y. Kim, Facile preparation and characterization of poly (vinyl alcohol) /chitosan/graphene oxide biocomposite nanofibers, J. Ind. Eng. Chem., 20 (2014) 4415–4420.

[18] D.C. Marcano, D.V. Kosynkin, J.M. Berlin, A. Sinitskii, Z. Sun, A. Slesarev, J.M. Tour, Improved synthesis of graphene oxide, ACS Nano., 4 (2010) 4806–4814.

[19] X.Y. Chen, Q.Q. Zhou, The production of porous carbon from calcium lignosulfonate without activation process and the capacitive performance, Electrochim. Acta, 71 (2012) 92–99.

[20] M. Yadav, K.Y. Rhee, I.H. Jung, S.J. Park, Eco-friendly synthesis, characterization and properties of a sodium carboxymethyl cellulose/graphene oxide nanocomposite film, Cellulose, 20(2) (2013) 687–698.

[21] W.K. Zhu, W. Li, Y. He, T. Duan, In-situ biopreparation of biocompatible bacterial cellulose/graphene oxide composites pellets, Appl. Surf. Sci., 338 (2015) 22–26.

[22] H. Mianehrow, M.H.M. Moghadam, F. Sharif, S. Mazinani, Graphene-oxide stabilization in electrolyte solutions using hydroxyethyl cellulose for drug delivery application, Int. J. Pharm., 484 (2015) 276–282.

[23] J. Yue, A.J. Epstein, Z. Zhong, P.K. Gallagher, A.G. MacDiarmid, Thermal stabilities of polyanilines, Synthetic Met., 41 (1991) 765–768.

[24] J. Yang, J.X. Wu, Q.F. Lü, T.T. Lin, Facile preparation of lignosulfonate–graphene oxide–polyaniline ternary nanocomposite as an effective adsorbent for Pb (II) ions, ACS Sustain. Chem. Eng., 2 (2014) 1203–1211.

[25] Z.L. Yao , N. Braidy, G.A. Botton, A. Adronov, Polymerization from the surface of single-walled carbon nanotubes–preparation and characterization of nanocomposites, J. Am. Chem. Soc., 125(51) (2003) 6015–1602.

[26] M.R. Loos, J. Yang, D.L. Feke, I. Manas-Zloczower, S. Unal, U. Younes, Enhancement of fatigue life of polyurethane composites containing carbon nanotubes, Compos. Part B- Eng., 44 (2013) 740–744.

[27] H. Luo, G. Xiong, Z. Yang, S.R. Raman, H. Si, Y. Wan, A novel three-dimensional graphene/bacterial cellulose nanocomposite prepared by in situ biosynthesis, RSC Adv., 4 (2014) 14369–14372.

[28] M. Xu, Q. Huang, X. Wang, R. Sun, Highly tough cellulose/graphene composite hydrogels prepared from ionic liquids, Ind. Crop. Prod., 70 (2015) 56–63.

[29] J. Shen, B. Yan, T. Li, Y. Long, N. Li, M. Ye, Study on graphene-oxide-based polyacrylamide composite hydrogels, Compos. Part A-Appl. Sci., 43 (2012) 1476–1481.

[30] S.H. Tu, C.X. Zhu, L.Y. Zhang, H.T. Wang, Q.G. Du, pore structure of macroporous polymers using polystyrene/silica composite particles as pickering stabilizers, Langmuir, 32(49) (2016) 13159–13166.

[31] H.Y. Xu, X.H. Zheng, Y.F. Huang, H.T. Wang, Q.G. Du, Interconnected porous polymers with tunable pore throat size prepared via pickering high internal phase emulsions, Langmuir, 32(1) (2015) 38–45.

[32] Y.Q. He, N.N. Zhang, X.D. Wang, Adsorption of graphene oxide/chitosan porous materials for metal ions, Chinese Chem. Lett., 22 (2011) 859–862.

[33] Q. Feng, F. Chen, X. Zhou, Preparation of thermo-sensitive hydrogels from acrylated lignin and N-isopropylacrylamide through photocrosslinking, J. Biobased Mater. Bio., 6 (2012) 336–342.

[34] S.T. Yang, S. Chen, Y. Chang, A. Cao, Y. Liu, H. Wang, Removal of methylene blue from aqueous solution by graphene oxide, J. Colloid Interf. Sci., 359 (2011) 24–29.

[35] L. Liu, Z.Y. Gao, X.P. Su, X. Chen, L. Jiang, J.M. Yao, Adsorption removal of dyes from single and binary solutions using a cellulose-based bioadsorbent, ACS Sustain. Chem. Eng., 3(3) (2015) 432–442.

[36] Y. Yao, F. Xu, M. Chen, Z. Xu, Z. Zhu, Adsorption behavior of methylene blue on carbon nanotubes, Bioresource Technol., 101 (2010) 3040–3046.

[37] Z. Wang, Y. Zhang, H. Pan, L. Tao, Adsorption of Methylene Blue on Organosolv Lignin from Rice Straw, Procedia Environ. Sci., 31 (2016) 3–11.

[38] L. Li, C. Luo, X. Li, H. Duan, X. Wang, Pareparation of magnetic ionic liquid/chitosan/graphene oxide composite and application for water treatment, Int. J. Biol. Macromol., 66 (2014) 172–178.